SUPPORTING INFORMATION

This Supporting Information is organized as follows: in Section **A** we provide details about the glass-forming models we employed in this work, and the preparation protocol used to generate our ensemble of glassy samples. In Section **B** the first-order expansion in temperature of an interaction energy is derived, from which the definition of a LTE $\mathcal{E}_\alpha$ emerges. We further explain how we calculate LTEs numerically, and discuss the generality of our results. In Section **C** we present distributions of the magnitude of forces between particles in our model glass. In Section **D** we describe how the LTE field is processed to give rise to soft spots and to predictions of ensuing plastic instabilities under shear. In Section **E** we explain how we quantify the level of predictiveness of the LTE field and describe how soft spot maps based on a normal-mode analysis are constructed.

A. MODELS AND PREPARATION PROTOCOLS

Models — We employ a single glass-forming model in two-dimensions (2D), and two glass-forming models in 3D, referred to as the 2DIPL, 3DIPL, and 3DKABLJ systems, respectively. The 2DIPL model is a 50:50 binary mixture of 'large' and 'small' particles of equal mass m, interacting via radially-symmetric purely repulsive inverse power-law pairwise potentials, that follow

$$\varphi(r_{ij}) = \begin{cases} \epsilon\left[\left(\frac{\lambda_{ij}}{r_{ij}}\right)^n + \sum_{\ell=0}^{q} c_{2\ell}\left(\frac{r_{ij}}{\lambda_{ij}}\right)^{2\ell}\right] & , \ \frac{r_{ij}}{\lambda_{ij}} \le x_c \\ 0 & , \ \frac{r_{ij}}{\lambda_{ij}} > x_c \end{cases}, \tag{A.1}$$

where r_{ij} is the distance between the i^{th} and j^{th} particles, ϵ is an energy scale, and x_c is the dimensionless distance for which φ_{IPL} vanishes continuously up to q derivatives. Distances are measured in terms of the interaction lengthscale λ between two 'small' particles, and the rest are chosen to be $\lambda_{ij}=1.18\lambda$ for one 'small' and one 'large' particle, and $\lambda_{ij}=1.4\lambda$ for two 'large' particles. The coefficients $c_{2\ell}$ are given by

$$c_{2\ell} = \frac{(-1)^{\ell+1}}{(2q-2\ell)!!(2\ell)!!}\frac{(n+2q)!!}{(n-2)!!(n+2\ell)}x_c^{-(n+2\ell)}. \tag{A.2}$$

We chose the parameters $x_c=1.48$, $n=10$, and $q=3$. The density was set to be $N/V=0.86\lambda^{-2}$; this choice sets the scale of characteristic $T=0$ interaction energies to be of order unity. We emphasize that this model glass-former does not lie in the proximity of an unjamming point since it possesses an intrinsic invariance to variations of density (or pressure), as established by the extensive work of Dyre et al. [1–3]. Indeed, none of the observables measured in our simulations or in our analysis depend on our particular choice of density. The 2DIPL model undergoes a computer-glass-transition at a temperature of $T_g \approx 0.5\epsilon/k_B$ for the density we chose.

The 3DIPL model is the three-dimensional version of the 2DIPL. Here we follow the same reasoning in setting the density and choose $N/V=0.82\lambda^{-3}$. The resulting glass transition temperature is $T_g \approx 0.52\epsilon/k_B$.

The 3DKABLJ is the canonical Kob-Andersen binary Lennard-Jones model [4]. It is a binary mixture of 80% type A particles and 20% type B particles of equal mass m, interacting via the following radially-symmetric pairwise potential

$$\varphi(r_{ij}) = \begin{cases} \varphi_{\text{LJ}}\left(\frac{r_{ij}}{\lambda_{ij}}\right) + \epsilon_{ij}\sum_{\ell=0}^{3} c_{2\ell}\left(\frac{r_{ij}}{\lambda_{ij}}\right)^{2\ell} & , \ \frac{r_{ij}}{\lambda_{ij}} \le x_c \\ 0 & , \ \frac{r_{ij}}{\lambda_{ij}} > x_c \end{cases}, \tag{A.3}$$

where $\varphi_{\text{LJ}}\left(\frac{r_{ij}}{\lambda_{ij}}\right) = 4\epsilon_{ij}\left[\left(\frac{r_{ij}}{\lambda_{ij}}\right)^{12} - \left(\frac{\lambda_{ij}}{r_{ij}}\right)^{6}\right]$ is the conventional Lennard-Jones potential. Energies are expressed in terms of the A-A interaction $\epsilon \equiv \epsilon_{AA}$, then $\epsilon_{AB}=1.5\epsilon$ and $\epsilon_{BB}=0.5\epsilon$. The interaction length parameters are expressed in terms of $\lambda \equiv \lambda_{AA}$, then $\lambda_{AB}=0.8$ and $\lambda_{BB}=0.88$. $x_c=2.5$ is the dimensionless distance for which φ vanishes continuously up to three derivatives. This condition sets the values of the coefficients $c_0=0.322042855424$, $c_2=-0.11564551766016$, $c_4=0.014774794872422$ and $c_4=-0.0006556954772111$. The density was set at $N/V=1.2$. With this parameter set the system undergoes a computer glass transition at $T_g \approx 0.45\epsilon/k_B$.

Preparation protocol — We prepared ensembles of glassy samples for all three models using the following protocol: first, systems were equilibrated in the high temperature liquid phase at $T=1.0\epsilon/k_B$. Then, the temperature was instantaneously set to a target value just below the respective T_g of each model, where the dynamics were ran for a duration $t_{\text{anneal}}=200\tau_0, 250\tau_0$ and $50\tau_0$ for the 2DIPL, 3DIPL and 3DKABLJ, respectively. Here $\tau_0 \equiv \sqrt{m}\lambda/\epsilon$ is the microscopic units of time. This short annealing step is necessary to avoid generating unphysical ultra-unstable glassy configurations that could occur in an instantaneous quench, and is computationally advantageous compared to a continuous quench at a fixed quench-rate. After the annealing step we minimized the energy to produce glassy samples by a standard conjugate gradient method. Using this protocol, we have generated 5000 independent glassy samples for all three models, with $N=10000$ for the 2DIPL system, and $N=2000$ for the 3DIPL and 3DKABLJ systems.

B. LOCAL THERMAL ENERGIES

In most of our work we omit particle indices with the goal of improving the clarity and readability of the text. We denote Nd-dimensional vectors as $\boldsymbol{v}$, each component

pertains to some particle index (e.g. i) and some Cartesian spatial component (e.g. ξ). Single, double and and triple contractions are denoted with $\cdot,:$, and $\vdots$, respectively. For example, the notation $\frac{\partial^3\mathcal{A}}{\partial\boldsymbol{x}\partial\boldsymbol{x}\partial\boldsymbol{x}}\vdots\boldsymbol{x}\boldsymbol{x}\boldsymbol{x}$ should be interpreted as $\sum_{ijk\xi\nu\upsilon}\frac{\partial^3\mathcal{A}}{\partial x_{i\xi}\partial x_{j\nu}\partial x_{k\upsilon}}x_{i\xi}x_{j\nu}x_{k\upsilon}$, where i,j,k run over particle indices and ξ,ν,υ run over Cartesian spatial components.

We begin with deriving an expression for the thermal average of a general observable $\mathcal{A}=\mathcal{A}(\boldsymbol{x})$ which depends on the coordinates $\boldsymbol{x}$, defined here as the displacement about an inherent state configuration. We denote with the superscript '(0)' quantities evaluated at the inherent state $\boldsymbol{x}=0$ (i.e. at zero temperature), e.g. $\mathcal{A}^{(0)}$, and $\mathcal{U}(\boldsymbol{x})$ denotes the potential energy.

The mean of the observable $\mathcal{A}$ is a function of temperature, defined as

$$\langle\mathcal{A}\rangle_{_T}\equiv\frac{\int\mathcal{A}(\boldsymbol{x})\exp\left(-\frac{\mathcal{U}(\boldsymbol{x})}{k_BT}\right)d\boldsymbol{x}}{\int\exp\left(-\frac{\mathcal{U}(\boldsymbol{x})}{k_BT}\right)d\boldsymbol{x}}=\frac{\int\mathcal{A}(\boldsymbol{x})\exp\left(-\frac{\delta\mathcal{U}(\boldsymbol{x})}{k_BT}\right)d\boldsymbol{x}}{\tilde{\mathcal{Z}}(T)}\,, \tag{B.1}$$

where $\delta\mathcal{U}\equiv\mathcal{U}-\mathcal{U}^{(0)}$ is the energy variation about the inherent state energy $\mathcal{U}^{(0)}$, and $\tilde{\mathcal{Z}}(T)\equiv\int\exp\left(-\frac{\delta\mathcal{U}(\boldsymbol{x})}{k_BT}\right)d\boldsymbol{x}$ is the relevant partition function. $\delta\mathcal{U}$ is expanded to third order in the coordinates as

$$\delta\mathcal{U}\simeq\tfrac{1}{2}\boldsymbol{\mathcal{M}}:\boldsymbol{x}\boldsymbol{x}+\tfrac{1}{6}\boldsymbol{\mathcal{U}}'''\vdots\boldsymbol{x}\boldsymbol{x}\boldsymbol{x}\,, \tag{B.2}$$

where $\boldsymbol{\mathcal{M}}\equiv\frac{\partial^2\mathcal{U}}{\partial\boldsymbol{x}\partial\boldsymbol{x}}$ is the dynamical matrix, and $\boldsymbol{\mathcal{U}}'''\equiv\frac{\partial^3\mathcal{U}}{\partial\boldsymbol{x}\partial\boldsymbol{x}\partial\boldsymbol{x}}$ is the third-order tensor of derivatives of the potential energy. In what follows we assume that the scale of characteristic fluctuations of the coordinates is set by the equipartition theorem, namely $\langle x^2\rangle\sim k_BT$, and therefore higher order products of coordinates are much smaller than k_BT. With this assumption, we expand the numerator of Eq. (B.1) as

$$\begin{aligned}\int\mathcal{A}(\boldsymbol{x})\exp\left(-\frac{\delta\mathcal{U}(\boldsymbol{x})}{k_BT}\right)d\boldsymbol{x}&\simeq\int\left(\mathcal{A}_0+\frac{\partial\mathcal{A}}{\partial\boldsymbol{x}}\cdot\boldsymbol{x}+\frac{1}{2}\frac{\partial^2\mathcal{A}}{\partial\boldsymbol{x}\partial\boldsymbol{x}}:\boldsymbol{x}\boldsymbol{x}\right)\exp\left(-\frac{\boldsymbol{\mathcal{M}}:\boldsymbol{x}\boldsymbol{x}}{2k_BT}\right)\left(1-\frac{\boldsymbol{\mathcal{U}}'''\vdots\boldsymbol{x}\boldsymbol{x}\boldsymbol{x}}{6k_BT}\right)d\boldsymbol{x}\\&\simeq\int\left(\mathcal{A}_0+\frac{1}{2}\frac{\partial^2\mathcal{A}}{\partial\boldsymbol{x}\partial\boldsymbol{x}}:\boldsymbol{x}\boldsymbol{x}-\frac{1}{6k_BT}\boldsymbol{x}\cdot\frac{\partial\mathcal{A}}{\partial\boldsymbol{x}}\boldsymbol{\mathcal{U}}'''\vdots\boldsymbol{x}\boldsymbol{x}\boldsymbol{x}\right)\exp\left(-\frac{\boldsymbol{\mathcal{M}}:\boldsymbol{x}\boldsymbol{x}}{2k_BT}\right)d\boldsymbol{x}\\&=\left(\mathcal{A}_0+\frac{k_BT}{2}\left[\frac{\partial^2\mathcal{A}}{\partial\boldsymbol{x}\partial\boldsymbol{x}}:\boldsymbol{\mathcal{M}}^{-1}-\frac{\partial\mathcal{A}}{\partial\boldsymbol{x}}\cdot\boldsymbol{\mathcal{M}}^{-1}\cdot\boldsymbol{\mathcal{U}}'''\vdots\boldsymbol{\mathcal{M}}^{-1}\right]\right)\int\exp\left(-\frac{\boldsymbol{\mathcal{M}}:\boldsymbol{x}\boldsymbol{x}}{2k_BT}\right)d\boldsymbol{x}\,,\end{aligned} \tag{B.3}$$

where we have used the identities

$$\int\boldsymbol{x}_i\boldsymbol{x}_j\exp\left(-\frac{\boldsymbol{\mathcal{M}}:\boldsymbol{x}\boldsymbol{x}}{2k_BT}\right)d\boldsymbol{x}=T\boldsymbol{\mathcal{M}}^{-1}_{ij}\int\exp\left(-\frac{\boldsymbol{\mathcal{M}}:\boldsymbol{x}\boldsymbol{x}}{2k_BT}\right)d\boldsymbol{x}\,,$$

$$\int\boldsymbol{x}_i\boldsymbol{x}_j\boldsymbol{x}_k\boldsymbol{x}_m\exp\left(-\frac{\boldsymbol{\mathcal{M}}:\boldsymbol{x}\boldsymbol{x}}{2k_BT}\right)d\boldsymbol{x}=T^2\left(\boldsymbol{\mathcal{M}}^{-1}_{ij}\boldsymbol{\mathcal{M}}^{-1}_{km}+\boldsymbol{\mathcal{M}}^{-1}_{ik}\boldsymbol{\mathcal{M}}^{-1}_{jm}+\boldsymbol{\mathcal{M}}^{-1}_{im}\boldsymbol{\mathcal{M}}^{-1}_{jk}\right)\int\exp\left(-\frac{\boldsymbol{\mathcal{M}}:\boldsymbol{x}\boldsymbol{x}}{2k_BT}\right)d\boldsymbol{x}\,.$$

Since $\tilde{\mathcal{Z}}(T)\simeq\left(1+\mathcal{O}(k_BT)\right)\int\exp\left(-\frac{\boldsymbol{\mathcal{M}}:\boldsymbol{x}\boldsymbol{x}}{2k_BT}\right)d\boldsymbol{x}$, we arrive at the result

$$\frac{\langle\mathcal{A}\rangle_{_T}-\mathcal{A}^{(0)}}{\frac{1}{2}k_BT}\simeq\frac{\partial^2\mathcal{A}}{\partial\boldsymbol{x}\partial\boldsymbol{x}}:\boldsymbol{\mathcal{M}}^{-1}-\frac{\partial\mathcal{A}}{\partial\boldsymbol{x}}\cdot\boldsymbol{\mathcal{M}}^{-1}\cdot\boldsymbol{\mathcal{U}}'''\vdots\boldsymbol{\mathcal{M}}^{-1}\,. \tag{B.4}$$

as appears in the main text. We stress that the effect of higher order derivatives of both $\mathcal{A}$ and $\mathcal{U}$ can also be explicitly calculated and is of a higher order in T (not shown).

In this work we study the local thermal energy (LTE), defined as follows: we focus on potential energy functions that can be written as a sum over pairwise interactions $\mathcal{U}=\sum_\alpha\varepsilon_\alpha$, where α labels the different pairs of interacting degrees of freedom. Using Eq. (B.4), we define the local thermal energy $\mathcal{E}_\alpha$ as

$$\begin{aligned}\mathcal{E}_\alpha&\equiv\lim_{T\to0}\frac{\langle\varepsilon_\alpha\rangle_{_T}-\varepsilon_\alpha^{(0)}}{\frac{1}{2}k_BT}\\&=\frac{\partial^2\varepsilon_\alpha}{\partial\boldsymbol{x}\partial\boldsymbol{x}}:\boldsymbol{\mathcal{M}}^{-1}-\frac{\partial\varepsilon_\alpha}{\partial\boldsymbol{x}}\cdot\boldsymbol{\mathcal{M}}^{-1}\cdot\boldsymbol{\mathcal{U}}'''\vdots\boldsymbol{\mathcal{M}}^{-1}\,.\end{aligned} \tag{B.5}$$

Examples of the LTE fields calculated in 2D model glasses can be found in Figs. 1 and 3 in the main text. These fields are calculated as follows: we perform a full diagonalization of the dynamical matrix $\boldsymbol{\mathcal{M}}$ calculated for each glassy sample, and obtain the complete set of eigenmodes $\{\boldsymbol{\Psi}_\ell\}_{\ell=1}^{N\hat{d}}$ and their associated eigenfrequencies $\{\omega_\ell\}_{\ell=1}^{N\hat{d}}$, where $\hat{d}$ is the spatial dimension. We then

solve the following linear equation for the thermal displacements $\boldsymbol{\mathcal{X}} \equiv -\boldsymbol{\mathcal{M}}^{-1}\cdot\boldsymbol{\mathcal{U}}''' : \boldsymbol{\mathcal{M}}^{-1}$ (see main text) using a conventional conjugate gradient solver

$$\boldsymbol{\mathcal{M}}\cdot\boldsymbol{\mathcal{X}} = -\sum_{\ell} \frac{\boldsymbol{\mathcal{U}}''' : \boldsymbol{\Psi}_\ell \boldsymbol{\Psi}_\ell}{\omega_\ell^2} \tag{B.6}$$

Expressions for $\boldsymbol{\mathcal{M}}$ and $\boldsymbol{\mathcal{U}}'''$ for pairwise potentials are available in e.g. [5]. Finally, the LTE $\mathcal{E}_\alpha$ is calculated for each interaction α as

$$\mathcal{E}_\alpha = \sum_{\ell} \frac{\frac{\partial^2 \varepsilon_\alpha}{\partial \boldsymbol{x}\partial \boldsymbol{x}} : \boldsymbol{\Psi}_\ell \boldsymbol{\Psi}_\ell}{\omega_\ell^2} + \frac{\partial \varepsilon_\alpha}{\partial \boldsymbol{x}} \cdot \boldsymbol{\mathcal{X}} \,. \tag{B.7}$$

The formalism presented above remains valid for systems in which the potential is written as a sum of 3-body (or higher) terms, e.g. [6]. In this case $\mathcal{U} = \sum_\alpha \varepsilon_\alpha$, where now α labels a *triple* of interacting particles. The same expression given in Eq. (B.5) would now describe the LTE associated with the triple α. A key point is that the forces

$$\boldsymbol{f}_\alpha \equiv \frac{\partial \varepsilon_\alpha}{\partial \boldsymbol{x}} \tag{B.8}$$

have a different form in the case of 3-body interactions compared to the case of pairwise interactions. In the latter, if the interaction is radially-symmetric, $\boldsymbol{f}_\alpha$ has the geometry of a dipole vector acting on the pair α, as illustrated in the left panel of Fig. 1. What is the form of $\boldsymbol{f}_\alpha$ for 3-body interactions? As an example, assume that the interaction $\varepsilon_\alpha = \varepsilon_\alpha(\theta_\alpha)$ depends upon the angle θ_α formed between a triple i, j, k of particles. In this case, $\boldsymbol{f}_\alpha$ is a field with the geometry as illustrated in the right panel of Fig. 1.

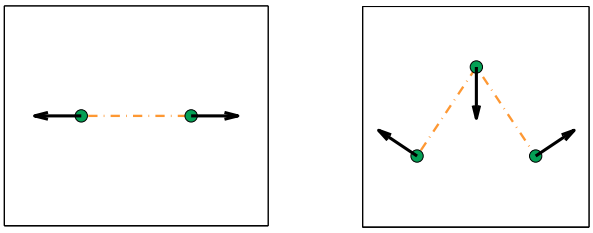

FIG. 1. Left panel: the geometry of $\boldsymbol{f}_\alpha$ in the case that ε_α is a pairwise radially-symmetric interaction. Right panel: same as left panel, for the case of a 3-body ε_α which depends on the angle between the triple of nodes.

We assert that as long as the interaction potential is translationally and rotationally invariant (i.e. it only depends on the relative distances and orientations between the triple α), the associated $\boldsymbol{f}_\alpha$ will be of a form which, when contracted with a slowly-varying field in space, will pick up contributions that are proportional to the spatial gradient of the slowly-varying field. The same reasoning also applies to contractions of slowly-varying fields with the third-order tensor $\boldsymbol{\mathcal{U}}'''$ as well. For these reasons, we expect LTEs to always filter out collective translational modes, and therefore be insensitive to the presence of low-frequency plane-waves, independently of the particular form of the potential energy.

Finally, we comment on the computational complexity of our numerical analysis: the bottleneck of the calculation is the requirement to obtain all the eigenmodes and eigenvalues of the dynamical matrix. The computational time of this full-diagonalization is known to scale as N^3. The computational time dedicated to the rest of the analysis is negligible compared to the diagonalization step. It is left for future research to investigate whether a partial diagonalization of the dynamical matrix (which would simply result in truncated sums in Eqs. (B.6) and (B.7)) would suffice for producing softness maps with comparable predictive powers to those obtained using a full diagonalization.

C. DISTRIBUTION OF FORCE MAGNITUDES

In the main text we present a scaling argument according to which the distribution of LTEs should follow $p(\mathcal{E}_\alpha) \sim \mathcal{E}_\alpha^{-9/4}$, based on the recent discovery that the asymptotic form of the distribution of glassy low-frequency modes in glassy systems follows $D_G(\omega) \sim \omega^4$ [7]. In this argument, we assume that the magnitudes of forces between the glass particles is narrowly distributed. Here, we present numerical evidence that validates this assumption: in Fig. 2 we present the distribution of the magnitude of pairwise forces between particles in the 3DIPL system, showing that it decays superexponentially at large values.

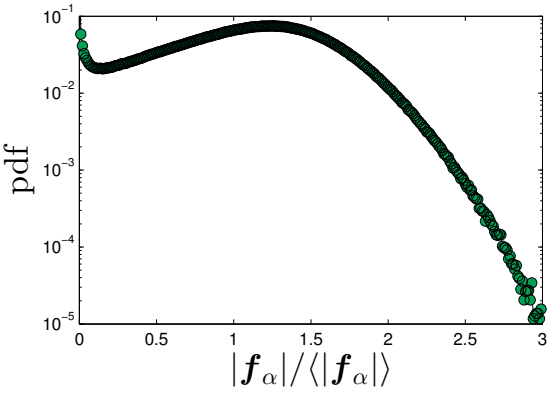

FIG. 2. The distribution of the magnitude of forces between particles measured for the 3DIPL system shows a superexponential decay at large values.

D. IDENTIFYING SOFT SPOTS AND THEIR DEGREE OF SOFTNESS

To quantitatively analyze the heterogenous spatial distribution of LTE $\mathcal{E}_\alpha$, we construct coarse-grained 2D map as follows. Space is discretized into bins of the smallest size which proved to always include at least two bonds' center of masses. In our case, it corresponds to a bin size of $1/40L$, with L being the linear size of the simulation box. The coarse-grained map is then built in two steps. In the first step, each bond is associated with a bin selected according to the bond's center of mass and the absolute value of its LTE contributes to the bin's value. In the second step, the map is smoothed out by averaging the bin's value with the values of all bins in the first layer of neighboring bins (8 bins in 2D). For easier processing, bonds with an associated LTE value smaller than $|\mathcal{E}_\alpha|=1.1$ were omitted. We verified that this choice does not affect the results, which are sensitive to large values of $|\mathcal{E}_\alpha|$.

The local maxima of the coarse-grained map were then extracted. These maxima are identified with soft spots, as described next. We first analyzed each row of the 2D maps at a time, where the bins corresponding to a local maximum were flagged. We repeated the same flagging procedure for every column. Bins which were flagged twice were defined as soft spots. As the exact location of the soft spot within the bin's area is of no interest, we define the soft spot location as the bin's coordinate with added white noise to avoid discretization effects. We used the bin's value as the soft spot score $\hat{\eta}$, which describes the average value of $|\mathcal{E}_\alpha|$ in the near vicinity of the soft spot center.

The LTE of bonds are widely distributed and consequently so are the scores of the soft spots, both within and between realizations. We therefore adopt the following standardized score

$$\Delta_{\mathcal{E}} = \frac{\eta_{\max}}{\hat{\eta}_i} \ , \tag{E.1}$$

where $\hat{\eta}_i$ is the score of the i^{th} soft spot and $\eta_{\max} = \max_i [\hat{\eta}_i]$ evaluated for each realization. Therefore, the softest spot in each realization has $\Delta_{\mathcal{E}}=1$ and not-as-soft spots are characterized by $\Delta_{\mathcal{E}}>1$, where the deviation from unity quantifies the degree of softness within each realization. This standardization allows a consistent numerical analysis per realization, as well as the calculation of distribution functions based on a large number of realizations. The analysis is based on 5000 independent realizations, where a few tens of soft spots were detected per realization. Among these spots, the softest ones — i.e. those with $\Delta_{\mathcal{E}}$ close to unity — dominate the plastic response under shearing. For example, there are on average 25 spots with $\Delta_{\mathcal{E}}\leq 2$, which according to Fig. 4 (left), predict nearly 70% of the first plastic events.

E. QUANTIFYING PREDICTIVENESS OF PLASTIC REARRANGEMENTS UNDER SHEAR

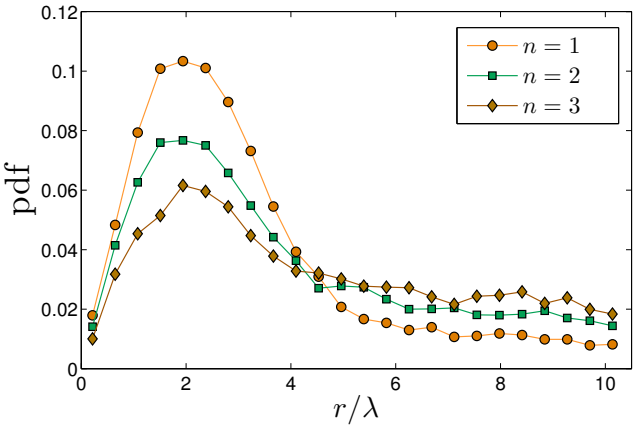

FIG. 3. The probability distribution function of the distance r (normalized by the bond-length between two small particles λ, cf. Eq. (A.1) and the text below it) between plastic events and the center of the nearest soft spot. It is observed that plastic events occur with high-probability close — within a few bond-lengths — to soft spots.

Plastic rearrangements — The performed athermal quasi-static shearing simulations followed well-established two-step protocols of first imposing an affine simple-shear transformation to the system and then minimizing its energy while enforcing Lees-Edwards boundary conditions, see e.g. [8–10]. During these simulations the energy was used as an indicator of plastic rearrangements/events which were identified with strain precision up to 10^{-6} using backtracking methods. The plastic events were automatically spatially localized by selecting the particle with the largest displacement value as a consequence of the energy minimization step at the occurrence of the plastic event.

Quantification — Each glass realization was sheared until 5 plastic events were triggered. The probability distribution function of the distance of plastic events to the nearest spot in space is shown in Fig. 3. It is observed that plastic events occur with high-probability near soft spots (corresponding to the peak around 2 bond-lengths). Consequently, we identify the soft spot which is closest to the k^{th} plastic event and record its standardized score $\Delta_{\mathcal{E}}$ for further analysis as described in the manuscript.

Normal-modes maps — To compare the LTE results with existing methods/results in the literature, we followed the protocol described in [11] to produce a field which is based on the 30 lowest normal-modes with non-vanishing associated energy. By constructing such normal-modes-based maps, each and every particle in the system has a score corresponding to a sum over the displacement squared of the modes. We then applied exactly the same protocol described in Section **D** in the context

of the LTE maps to the normal-modes-based maps, where bonds' centers of mass were replaced with particle positions and the LTE absolute values of bonds were replaced with particles' scores. The results of the comparison are presented in the main text.

[1] Bailey NP, Pedersen UR, Gnan N, Schrder TB, Dyre JC (2008) Pressure-energy correlations in liquids. i. results from computer simulations. *J. Chem. Phys.* 129(18):184507.

[2] Dyre JC (2016) Simple liquids quasiuniversality and the hard-sphere paradigm. *Journal of Physics: Condensed Matter* 28(32):323001.

[3] Bacher AK, Schrøder TB, Dyre JC (2014) Explaining why simple liquids are quasi-universal. *Nat. Commun.* 5.

[4] Kob W, Andersen HC (1995) Testing mode-coupling theory for a supercooled binary lennard-jones mixture i: The van hove correlation function. *Phys. Rev. E* 51(5):4626–4641.

[5] Karmakar S, Lerner E, Procaccia I (2010) Athermal nonlinear elastic constants of amorphous solids. *Phys. Rev. E* 82(2):026105.

[6] Stillinger FH, Weber TA (1985) Computer simulation of local order in condensed phases of silicon. *Phys. Rev. B* 31(8):5262–5271.

[7] Lerner E, Düring G, Bouchbinder E (2016) Statistics and properties of low-frequency vibrational modes in structural glasses. *Phys. Rev. Lett.* 117(3):035501.

[8] Maloney C, Lemaître A (2004) Subextensive scaling in the athermal, quasistatic limit of amorphous matter in plastic shear flow. *Phys. Rev. Lett.* 93(1):016001.

[9] Maloney CE, Lemaître A (2006) Amorphous systems in athermal, quasistatic shear. *Phys. Rev. E* 74(1):016118.

[10] Karmakar S, Lerner E, Procaccia I, Zylberg J (2010) Statistical physics of elastoplastic steady states in amorphous solids: Finite temperatures and strain rates. *Phys. Rev. E* 82(3):031301.

[11] Widmer-Cooper A, Perry H, Harrowell P, Reichman DR (2008) Irreversible reorganization in a supercooled liquid originates from localized soft modes. *Nature Phys.* 4(9):711–715.